Numerical Study on Steady and Transient Mass/Heat Transfer Involving a Liquid Sphere in Simple Shear Creeping Flow

Run Li, Jingsheng Zhang, Chao Yang, and Zai-Sha Mao
National Key Laboratory of Biochemical Engineering, Key Laboratory of Green Process and Engineering, Institute of Process Engineering, Chinese Academy of Sciences, Beijing 100190, China

Xiaolong Yin
Dept. of Petroleum Engineering, Colorado School of Mines, Golden, CO 80402

DOI 10.1002/aic.14239
Published online October 4, 2013 in Wiley Online Library (wileyonlinelibrary.com)

A numerical method is utilized to examine the steady and transient mass/heat transfer processes that involve a neutrally buoyant liquid sphere suspended in simple shear flow at low Reynolds numbers is described. By making use of the known Stokes velocity field, the convection-diffusion equations are solved in the three-dimensional spherical coordinates system. For the mass transfer either outside or inside a liquid sphere, Sherwood number Sh approaches an asymptotic value for a given viscosity ratio at sufficiently high Peclet number Pe. In terms of the numerical results obtained in this work, two new correlations are derived to predict Sh at finite Pe for various viscosity ratios. © 2013 American Institute of Chemical Engineers *AIChE J*, 60: 343–352, 2014
Keywords: mass transfer, shear flow, drop, numerical simulation, transport processes

Introduction

Multiphase systems exist extensively in natural and industrial processes. Dispersed phases, such as bubbles, liquid droplets, and solid particles, would translate and rotate in flow fields; inclusion of a dispersed phase makes modeling of transport and chemical reactions more complicated. Among others, the study on the behavior of a single bubble, drop, or particle has a fundamental significance to the industrial scale-up. There have been many investigations on the translation and mass/heat transfer of a single particle in uniform flows.[1,2] In contrast, the studies are insufficient on the transport process around a bubble, drop, or particle in shear flow. As shear flow is expected in practically all chemical reactors and particularly in stirred tanks, understanding the transport around a dispersed phase in shear flow is of great importance. The rotation of a spherical liquid drop in simple shear flow, and the transport processes associated with this motion are the focus of this work.

Frankel and Acrivos[3] and Acrivos[4] studied the rates of heat and mass transfer from small cylinders and solid spheres in simple shear flow in the lower limit of Reynolds number $Re \to 0$ by the singular perturbation method. When the direction of the flux is from the particle to infinite bulk phase, they derived the asymptotic formulas which related the Nusselt number Nu to the Peclet number Pe in the limit of $Pe \to 0$, where the Nusselt number is $Nu=ha/K_t$, the Peclet number $Pe=\dot{\gamma}a^2/D$ ($Pe=\dot{\gamma}a^2/\alpha$ for heat transfer), h the heat transfer coefficient, K_t the thermal conductivity, $\dot{\gamma}$ the characteristic magnitude of the velocity gradient, D the mass diffusivity, α the thermal diffusivity, and a the sphere radius. For the heat transfer from a cylinder, they found Nusselt number approached a asymptotic value ($Nu \approx 2.865$) at $Pe \to \infty$, whereas it is 4.5 for a solid sphere.

Robertson and Acrivos[5,6] considered experimentally the momentum and heat transfer from a cylinder immersed in a uniform shear field. Because the closed streamlines surrounded the freely rotating cylinder, the asymptotic Nusselt number was found to be 2.65, in reasonable agreement with the theoretical value of 2.865 obtained by Frankel and Acrivos.[3]

Subramanian and Koch[7,8] and Subramanian et al.[9] found that the microscale inertia would break the closed streamlines near a solid sphere immersed in a simple shear flow, leading to the deviation from the Stokes asymptote. Through a boundary layer analysis, they arrived at a correlation $Nu=\left(0.325-0.126Re^{1/2}\right)(RePe)^{1/3}+O(1)$ in the limit of $Re \ll 1$ and $PeRe \gg 1$.

Yang et al.[10] applied the boundary layer analysis method coupled with numerical simulation to solve the transport process from a solid sphere suspended in simple shear flow at large Pe and $Re \leq 10$. Their numerical results at high Pe and $Re \ll 1$ were consistent with the theoretical results derived by Subramanian and Koch.[7,8] When $Re \to 0$, their Nusselt number at high Pe also approached the asymptotic value of 4.5, in agreement with Acrivos' analysis.[4]

For a spherical drop in simple shear creeping flow, Leal[11] used a perturbation method to calculate the temperature field in both phases in the limit of $Pe \to 0$. Here, the far field is a linear temperature profile with a gradient normal to the velocity at far upstream and downstream boundaries. The final result is an expression for evaluating the effective thermal conductivity of a dilute suspension. Li et al.[12] found the

Correspondence concerning this article should be addressed to C. Yang at chaoyang@home.ipe.ac.cn.

spiraling streamline structure at the 2-D plane near a liquid sphere immersed in a simple shear flow at low and moderate *Re* by numerical method.

The streamlines outside a drop are open in uniform flows.[1] Such a pattern of the streamlines will lead to Sherwood number *Sh* increasing with increasing Peclet number, where the Sherwood number is $Sh=ka/D$ and k is the mass transfer coefficient. Aforementioned findings reveal that there is a significant difference between the shear flow case and the uniform flow one. If theoretical analysis is used to investigate the transport process of a single sphere immersed in simple shear creeping flow, the range of *Pe* is restricted to either very low or infinite values. Most previous research works on drops in shear flow were focused on the particle motion[13,14] and the transport process of a dilute suspension.[11] Limited information has been reported concerning the characteristics of mass/heat transfer from or to a drop in simple shear flow, particularly at large *Pe*.

In this work, the convection-diffusion equation is solved by a finite difference method[15] in order to examine the solute concentration near the surface of a fluid sphere immersed in simple shear creeping flow over a range of Peclet numbers; such results of mass transfer have not been previously reported. The validity of the numerical method was checked by computing the rate of heat/mass transfer of a translating drop.

Model Description

Flow field of simple shear creeping flow around a liquid sphere

The particular flow to be studied here corresponds to one that surrounds a neutrally buoyant liquid sphere of radius a; far from the liquid sphere, the unperturbed flow is a simple shear, which is represented in the Cartesian coordinates by

$$\mathbf{u}_\infty=\mathbf{E}\cdot\mathbf{r},\quad \boldsymbol{\Gamma}=\begin{pmatrix}0&1&0\\0&0&0\\0&0&0\end{pmatrix}\dot{\gamma},\quad \mathbf{E}=\begin{pmatrix}0&\frac{1}{2}&0\\\frac{1}{2}&0&0\\0&0&0\end{pmatrix}\dot{\gamma},$$
$$\boldsymbol{\Omega}=\begin{pmatrix}0&\frac{1}{2}&0\\-\frac{1}{2}&0&0\\0&0&0\end{pmatrix}\dot{\gamma} \tag{1}$$

where $\mathbf{r}$ is the position vector, Γ is the transpose of the velocity gradient tensor, and $\mathbf{E}$ and $\boldsymbol{\Omega}$ are the rate-of-strain tensor and the vorticity tensor, respectively. In this work, the spherical coordinate system and flow direction of the ambient phase are illustrated in Figure 1.

The velocity field in the creeping flow regime caused by the inclusion of a liquid sphere has been well documented[16] and given by

$$\mathbf{u}_1=\boldsymbol{\Gamma}\cdot\mathbf{r}-\frac{\lambda}{(\lambda+1)r^5}\mathbf{E}\cdot\mathbf{r}-\left[\frac{(5\lambda+2)}{2(\lambda+1)}\frac{1}{r^5}-\frac{5\lambda}{2(\lambda+1)}\frac{1}{r^7}\right](\mathbf{r}\cdot\mathbf{E}\cdot\mathbf{r})\mathbf{r} \tag{2}$$

$$\mathbf{u}_2=\boldsymbol{\Omega}\cdot\mathbf{r}+\left[-\frac{3}{2(\lambda+1)}+\frac{5\lambda^2}{2(\lambda+1)}\right]\mathbf{E}\cdot\mathbf{r}-\frac{1}{(\lambda+1)}(\mathbf{r}\cdot\mathbf{E}\cdot\mathbf{r})\mathbf{r} \tag{3}$$

where λ is the viscosity ratio of the dispersed phase to the continuous phase, and subscript 1 refers to the continuous phase and 2 the dispersed phase. In a spherical coordinate system

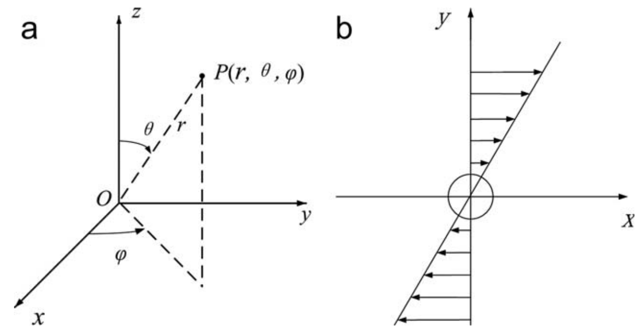

Figure 1. The spherical coordinate system and the flow direction of ambient phase in this work.

(a) Spherical coordinate system; (b) Flow direction of ambient phase.

(r,θ,φ) with the liquid sphere centered at the origin, scaling Eqs. 2 and 3 by $\dot{\gamma}a$, the dimensionless velocity components are

$$u_{1r}=\sin^2\theta\sin\varphi\cos\varphi\left(r-\frac{5\lambda+2}{2(\lambda+1)}\frac{1}{r^2}+\frac{3\lambda}{2(\lambda+1)}\frac{1}{r^4}\right) \tag{4}$$

$$u_{1\theta}=\sin\theta\cos\theta\sin\varphi\cos\varphi\left(r-\frac{\lambda}{\lambda+1}\frac{1}{r^4}\right) \tag{5}$$

$$u_{1\varphi}=-r\sin\theta\sin^2\varphi-\frac{\lambda}{2(\lambda+1)}\frac{1}{r^4}\sin\theta\left(\cos^2\varphi-\sin^2\varphi\right) \tag{6}$$

$$u_{2r}=\sin^2\theta\sin\varphi\cos\varphi\left(-\frac{3r}{2(\lambda+1)}+\frac{3r^3}{2(\lambda+1)}\right) \tag{7}$$

$$u_{2\theta}=\sin\theta\cos\theta\sin\varphi\cos\varphi\left(-\frac{3r}{2(\lambda+1)}+\frac{5r^3}{2(\lambda+1)}\right) \tag{8}$$

$$u_{2\varphi}=-\frac{1}{2}r\sin\theta+\left(-\frac{3r}{4(\lambda+1)}+\frac{5r^3}{4(\lambda+1)}\right)\sin\theta\left(\cos^2\varphi-\sin^2\varphi\right) \tag{9}$$

Figure 2 depicts the topology of streamlines on the x-y plane ($\theta=\pi/2$) both outside and inside a liquid sphere in simple shear flow at several viscosity ratios. Apparently, a set of closed streamlines surrounds the suspended drop in the creeping flow regime and extends to $\pm\infty$ along the x-axis. Nevertheless, for sufficiently large values of $|y|$, open streamlines also exist further away because of the diminishing hydrodynamic disturbance from the drop. The shear stress from the continuous phase generates circulations inside the liquid sphere. The smaller the viscosity ratio (less viscous drop), the more strong circulation is caused by the shear stress. It is observed that the value of λ has a significant influence on the topology of streamlines inside a drop. Specifically, it is observed that a single circulation is formed at $\lambda=1$ and $\lambda=10$, the shape of which is nearly circular for $\lambda=10$ and oval for $\lambda=1$. The single circulation cell splits into two circulation cells at $\lambda=0.1$.

Governing equations for mass/heat transfer

Making use of the known velocity field (Eqs. 4–9), the concentration field can be examined by solving the general transient advection-diffusion equation outside and inside the drop

$$\frac{\partial c_i}{\partial t}+\mathbf{u}_i\cdot\nabla c_i=D_i\nabla^2 c_i \tag{10}$$

where c is the concentration of solute, D is the mass diffusivity, and the subscript refers to the continuous phase

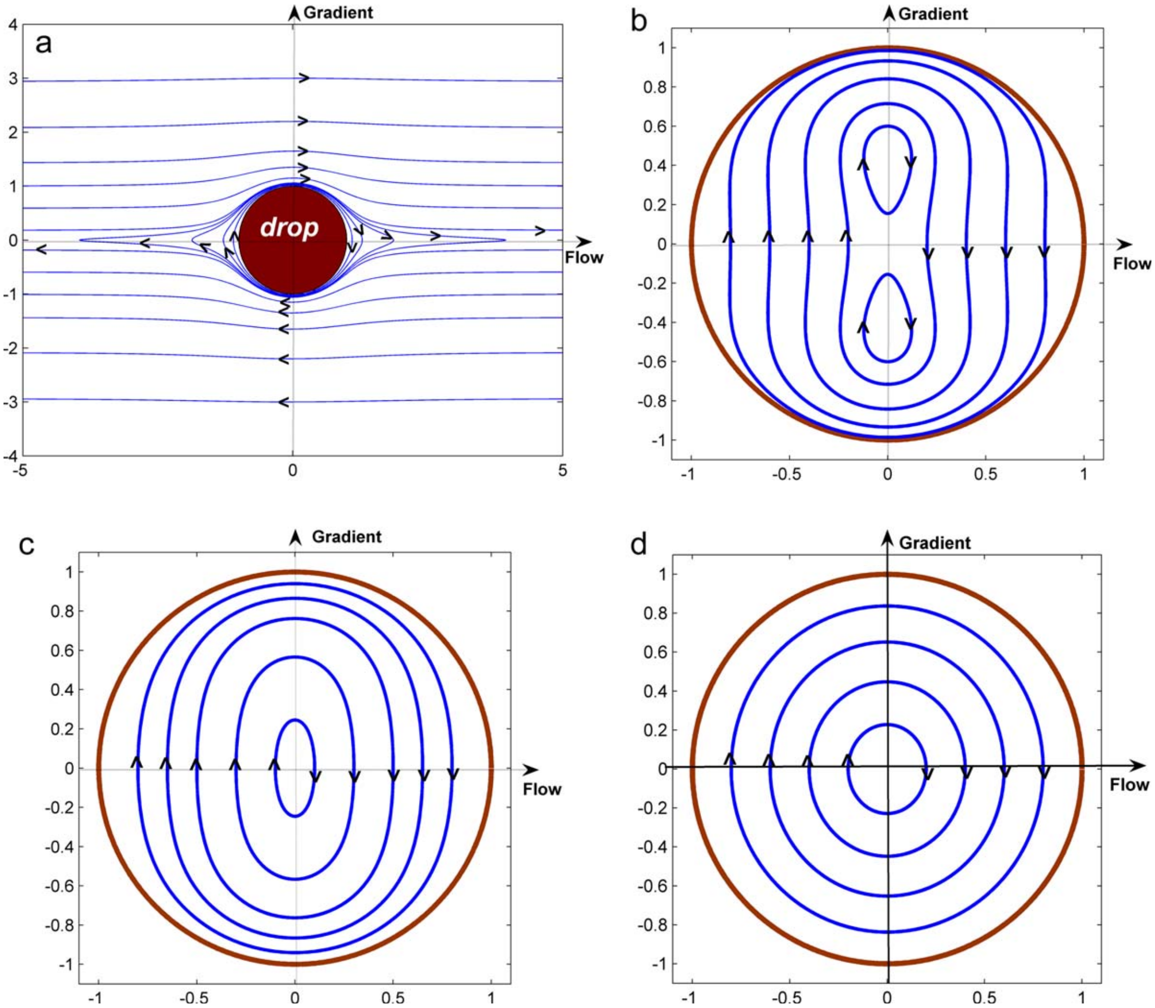

Figure 2. Flow field for a liquid sphere immersed in simple shear creeping flow on the *x-y* plane.

(a) Streamlines outside a liquid sphere at $\lambda = 1$; (b) Streamlines inside a liquid sphere at $\lambda = 0.1$; (c) Streamlines inside a liquid sphere at $\lambda = 1$; (d) Streamlines inside a liquid sphere at $\lambda = 10$. [Color figure can be viewed in the online issue, which is available at wileyonlinelibrary.com.]

(i = 1) and the liquid sphere (i = 2). When temperature is considered as a passive scalar and the effect of viscous heating is neglected, the energy equation governing the temperature distributions would obey an equation of the same nature. Thus, there is no need to address heat transfer separately.

Some common assumptions are adopted here to simplify the problem: (1) the surface tension between the two phases is sufficiently high so that the shape of the liquid drop is spherical; (2) mass transfer does not affect the net volume of the liquid sphere; (3) the physical properties of two phases are uniform and constant; (4) both fluid phases are Newtonian; and (5) there is no liquid–liquid interface resistance to mass transfer. Under these assumptions, the dimensionless model equation (Eq. 11) expressed in a spherical coordinate system (r,θ,φ) is

$$\frac{\partial C_i}{\partial \tau}+\frac{1}{r^2}\frac{\partial}{\partial r}\left(r^2 u_{ir} C_i\right)+\frac{1}{r\sin\theta}\frac{\partial}{\partial\theta}\left(u_{i\theta}\sin\theta C_i\right)+\frac{1}{r\sin\theta}\frac{\partial}{\partial\varphi}\left(u_{i\varphi}C_i\right)$$
$$=\frac{1}{Pe_i}\left[\frac{1}{r^2}\frac{\partial}{\partial r}\left(r^2\frac{\partial C_i}{\partial r}\right)+\frac{1}{r\sin\theta}\frac{\partial}{\partial\theta}\left(\frac{1}{r}\sin\theta\frac{\partial C_i}{\partial\theta}\right)+\frac{1}{r\sin\theta}\frac{\partial}{\partial\varphi}\left(\frac{1}{r\sin\theta}\frac{\partial C_i}{\partial\theta}\right)\right] \tag{11}$$

where $\tau=\dot{\gamma}t$ is the dimensionless time, and C_i is the dimensionless concentration.

We consider two mass transfer situations. The first situation is the steady-state mass transfer outside a liquid sphere. The internal circulation is assumed quick enough to assure that concentration is equilibrated, and mass transfer does not lower the solute concentration in the sphere. The dimensionless concentration is defined by $C_1=(c_1-c_\infty)/(c_1^s-c_\infty)$, and the boundary conditions[17] are

$$r=1,\quad C_1=C_1^s=1 \tag{12}$$

$$r\rightarrow\infty,\quad C_1=C_\infty=0 \tag{13}$$

The second situation is the unsteady mass transport inside the drop, the limit case when the external circulation is very quick and the internal transport is slow.

The initial concentration of the drop, c_0, is higher than that of the main stream. So C_2 is defined as $(c_0-c_2)/(c_0-c_2^s)$, and the boundary and initial conditions[16] are

$$\tau\geq 0\quad\text{and}\quad r=1,\quad C_1=C_2^s=0 \tag{14}$$

$$\tau=0\quad\text{and}\quad r\leq 1,\quad C_2=1 \tag{15}$$

At the center of the droplet, the concentration is continuous[18]

$$r=0, \quad C_1(i_0,j_0,k_0)=\frac{1}{N_\theta+N_\varphi}\sum_{j=1}^{N_\theta}\sum_{k=1}^{N_\varphi}C_1(i_0+1,j,k) \quad (16)$$

For both the external and internal transport processes, the concentration is also continuous at the z-axis[18]

$$\theta=0 \quad \text{or} \quad \theta=\pi, \quad C_1(i_0,j,k_0)=\frac{1}{N_\varphi}\sum_{k=1}^{N_\varphi}C_1(i_0+1,j,k) \quad (17)$$

In the φ direction, the concentration is also continuous so that the periodic condition applies.

Scheme of numerical simulation

In this study, the advection-diffusion equation is solved by the finite difference method. A fifth-order weighted essentially nonoscillatory scheme in the convective term, a central difference scheme in the diffusion term and a third-order total variation diminishing Runge-Kutta scheme in the time evolution are adopted in solving Eq. 11 with sufficient accuracy.[15]

The computational domain is $0 \le r \le R$, $0 \le \theta \le \pi$ and $0 \le \varphi \le 2\pi$, where R is the size of the computing domain in the radial direction. The governing Eq. 11 is discretized on a grid, which is uniform in the azimuthal (φ) and the polar (θ) directions, but nonuniform in the radial (r) direction. For the grid in the continuous phase, 20–30 nodes in the r direction were set tight and uniform near the surface of the sphere because the concentration boundary is very thin, but after that an exponential expansion of grid spacing, $r(i)=r(i-1)e^{\beta}$, was applied, where β is a small constant used to adjust the grid spacing. For the grid in the liquid drop, there are also 10–20 nodes densely and uniformly in the r direction near the sphere surface, whereas the nodes away from the surface are uniform but with a larger grid spacing. For the external transport problem, the radial location where the far field boundary condition, Eq. 13, is approximately imposed could affect the numerical result. The independence of simulation results on the radial location was tested on four values of R ($R=10a$, $30a$, $60a$, and $110a$). Our simulations show that $R=60a$ is reasonable for computational accuracy. For both the external and internal transport processes, the overall Sherwood number is used to represent the mass transfer rate and given by

$$Sh=\frac{a^2}{4\pi\Delta C_i}\int_{\theta=0}^{\theta=\pi}\int_{\varphi=0}^{\varphi=2\pi}\left(-\frac{\partial C}{\partial r}\bigg|_{r=1}\right)\sin\theta \mathrm{d}\theta\mathrm{d}\varphi \quad (18)$$

where $\Delta C_1=C_1^{\mathrm{s}}-C_\infty=1$ and $\Delta C_2=C_2^{\mathrm{s}}-\overline{C}_{\mathrm{d}}$ are the driving forces for heat/mass transfer in the two cases, and $\overline{C}_{\mathrm{d}}$ is the dimensionless average concentration of the sphere that can be calculated by

$$\overline{C}_{\mathrm{d}}=\frac{\int_0^1\int_0^\pi C_2 r^2\sin\theta \mathrm{d}r\mathrm{d}\theta}{\int_0^1\int_0^\pi r^2\sin\theta \mathrm{d}r\mathrm{d}\theta}=\frac{3}{2}\int_0^1\int_0^\pi C_2 r^2\sin\theta \mathrm{d}r\mathrm{d}\theta \quad (19)$$

For the solid sphere,[10] the smallest dimensionless mesh size in the radial direction next to the drop surface is ensured less than $O(Pe^{-1/3})$. In this work, we follow the same procedure. Figures 3 and 4 represent the grid convergence for the first-order derivative of the scalar on the surface of drop for both internal and external problems. We could found $\Delta r=5\times10^{-4}$ is sufficient in the steady problem for Peclet number up to 100,000 and the transient one for Peclet number up to 50,000, where Δr presented is the smallest grid spacing near the surface.

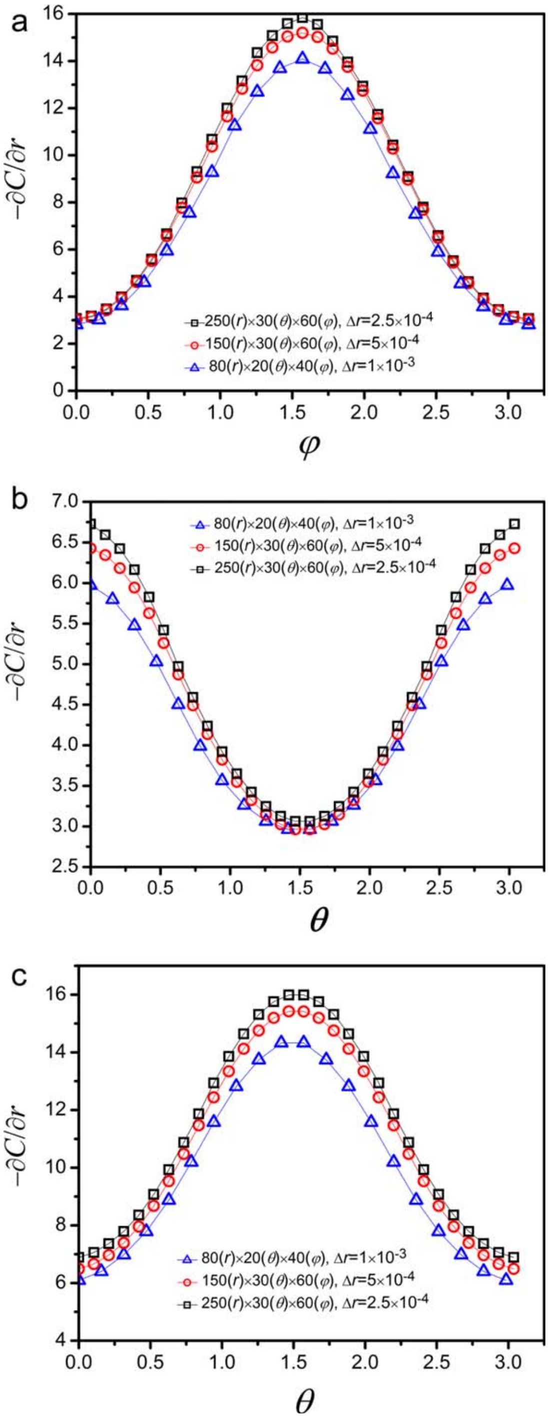

Figure 3. Grid convergence for the first-order derivative of scalar *C* on the surface of a drop for external problem (*Pe* = 100,000, λ=1).

(a) $\theta=\pi/2$; (b) $\varphi=0$; (c) $\varphi=\pi/2$. [Color figure can be viewed in the online issue, which is available at wileyonlinelibrary.com.]

For the steady transport process from a liquid sphere in simple shear creeping flow, a sample of our numerical results is presented in Table 1. It shows the asymptotic Sh values at $\lambda=1$ for several Pe values calculated on three discretization meshes. The grid sensitivity analysis reveals that an accurate solution is obtained by using a grid of

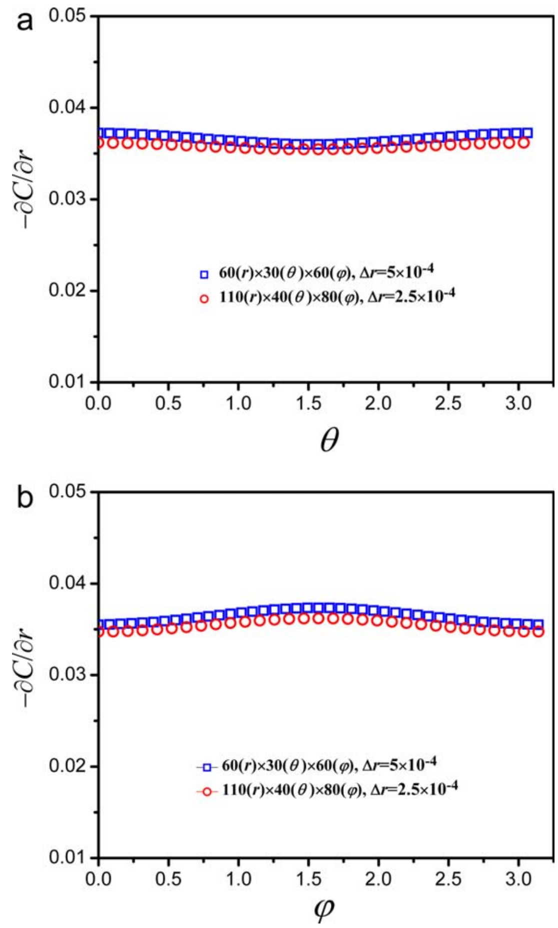

Figure 4. Grid convergence for the first-order derivative of scalar C on the surface of a drop for internal problem ($Pe = 100{,}000$, $\lambda = 100$, $\overline{C}_d = 0.01$).

(a) $\varphi = 0$; (b) $\theta = \pi/2$. [Color figure can be viewed in the online issue, which is available at wileyonlinelibrary.com.]

$150(r) \times 30(\theta) \times 60(\varphi)$ ($\Delta r = 0.0005$ and $R = 60$) at Pe_1 up to 100,000.

For the transient transport process inside a liquid sphere in simple shear creeping flow, a grid of $60(r) \times 30(\theta) \times 60(\varphi)$ ($\Delta r = 0.0005$) is sufficient for computing the unsteady internal mass transfer in the range of $10 \leq Pe_2 \leq 50{,}000$. A sample of our numerical results is presented in Table 2 at $\lambda = 1$.

Results and Discussion

Validation of numerical scheme

In order to verify the reliability and accuracy of the numerical method used in this study, both the external and internal mass transfer of a translating liquid sphere in creeping flow are solved first by using the same three-dimensional numerical scheme as described earlier. For the steady transport outside a translating liquid sphere at low Reynolds numbers, Feng et al.[19] solved the transport equations numerically and their results agreed well with the experimental data by Bowman et al.[20] Clift et al.[1] used the boundary layer theory to deduce the following correlation

$$Sh = 0.460\sqrt{Pe/(1+\lambda)} \tag{20}$$

This approximation applies if $Re \ll 1$ and $Pe \gg 1.2(3\lambda+1)^2(1+\lambda)$. We use the known velocity field[1] to calculate the mass transfer rate. The comparison between present results and those in the published literature[1,19] is shown in Figure 5. As can be seen in Figure 5a, our simulations at low Pe_1 is in good agreement with the results of Feng et al.[18] And Figure 5b shows that our result also agrees well with Clift et al.[1] as Peclet number increases.

For the transient internal transfer inside a translating liquid sphere, Sh would decrease with increasing time and reach an asymptotic value after sufficient time is lapsed. The asymptote comes from the fact that both the concentration gradient on the drop surface and the driving force decrease in proportion. Newman[21] and Kronig and Brink[22] obtained the following relations

$$Sh_2 \to 3.29 \quad (Pe \to 0) \tag{21}$$

$$Sh_2 \to 8.83 \quad (Pe \to \infty) \tag{22}$$

Juncu[23] studied the same problem by numerical simulation. A comparison between our results and Juncu's is shown in Figure 6, which indicates the consistency of both studies. The results presented in Figures 5 and 6 reveal that our numerical scheme is reliable and accurate enough in dealing with the mass/heat transfer problems on a circulating liquid sphere.

Mass transfer outside a liquid sphere

Figure 7 reveals that the lower the viscosity ratio, the higher the radial velocity component near the surface of a

Table 2. Mesh Behavior of Sh at Various Pe_2 and $\lambda = 1$ for Internal Problem in Simple Shear Flow

	Sherwood Number (Sh)	
Pe_2	$60(r) \times 30(\theta) \times 60(\varphi)$ ($\Delta r = 0.0005$)	$110(r) \times 40(\theta) \times 80(\varphi)$ ($\Delta r = 0.00025$)
10	3.2910	3.3082
100	3.3672	3.4095
500	3.4910	3.5423
1000	3.5300	3.5877
5000	3.5722	3.6397
10,000	3.5785	3.6518
50,000	3.5880	3.6636

Table 1. Mesh Behavior of Sh at Various Pe_1 and $\lambda = 1$ for External Problem in Simple Shear Flow

	Sherwood Number (Sh)		
Pe_1	$80(r) \times 20(\theta) \times 40(\varphi)$ ($\Delta r = 0.001$, $R = 40$)	$150(r) \times 30(\theta) \times 60(\varphi)$ ($\Delta r = 0.0005$, $R = 60$)	$250(r) \times 30(\theta) \times 60(\varphi)$ ($\Delta r = 0.00025$, $R = 80$)
10	2.012	2.051	2.062
100	3.544	3.649	3.695
1000	5.502	5.750	5.856
5000	6.965	7.212	7.319
10,000	7.283	7.558	7.641
50,000	7.845	8.048	8.137
100,000	7.870	8.068	8.165

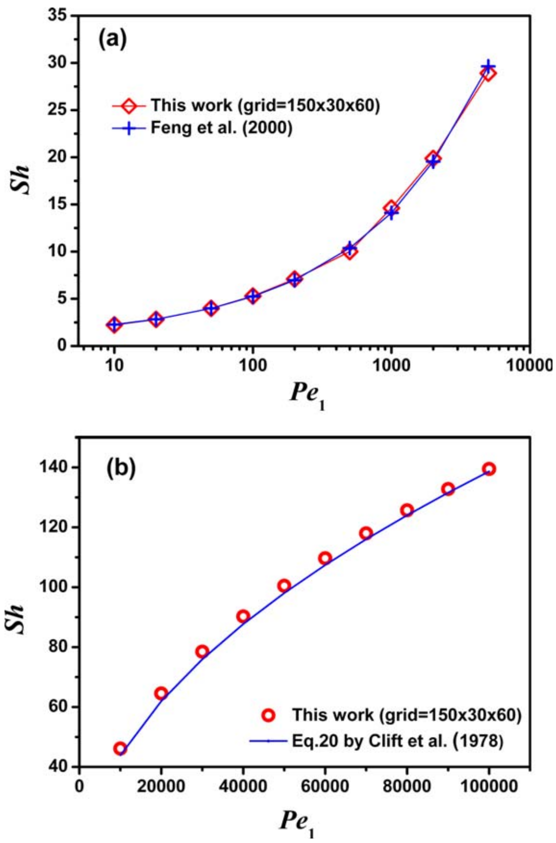

Figure 5. Steady transport behavior for a translating liquid sphere at $\lambda = 0.1$ in creeping flow using a grid of $150(r) \times 30(\theta) \times 60(\varphi)$ ($\Delta r = 0.0005$, and $R = 60$).

(a) Variation of Sh with Pe_1 (10–5000); (b) Variation of Sh with Pe_1 (10,000–100,000). [Color figure can be viewed in the online issue, which is available at wileyonlinelibrary.com.]

liquid sphere. For the steady-state transport problem, Figure 8 shows the effect of the Peclet number on the variation of Sh at several viscosity ratios. Different asymptotes of the Sherwood number were identified. Figure 8 indicates the larger the viscosity ratio, the smaller the velocity and the rate of

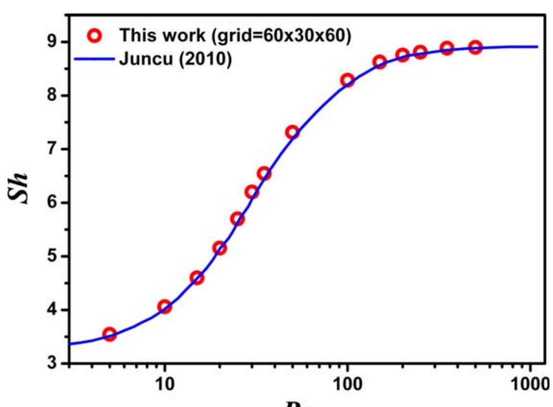

Figure 6. Unsteady transport behavior inside a translating liquid sphere at $\lambda = 1$ in creeping flow using a grid of $60(r) \times 30(\theta) \times 60(\varphi)$ ($\Delta r = 0.0005$).

[Color figure can be viewed in the online issue, which is available at wileyonlinelibrary.com.]

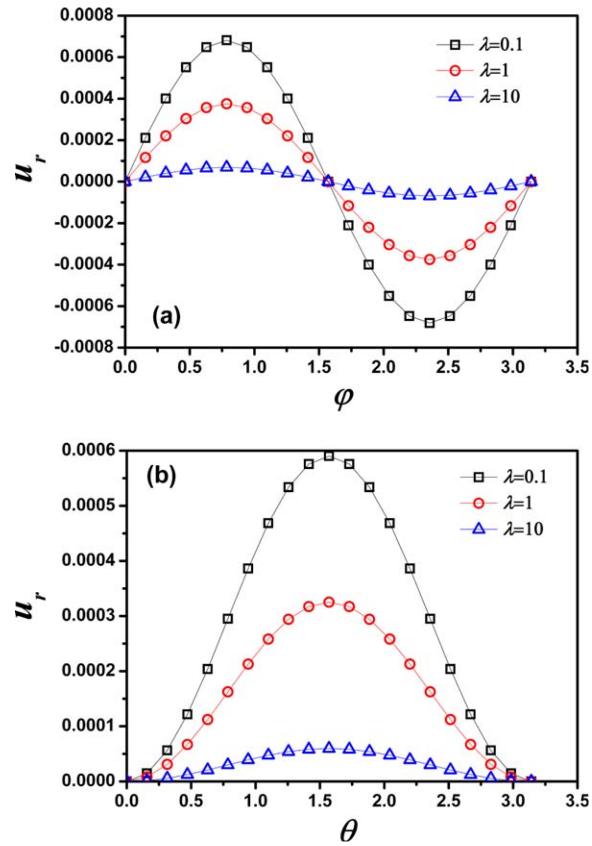

Figure 7. Variation of velocity normal to the surface at $r = 1.0005$ as a function of the angles (φ and θ) for different viscosity ratios.

(a) $\theta = \frac{\pi}{2}$; (b) $\varphi = \frac{\pi}{3}$. [Color figure can be viewed in the online issue, which is available at wileyonlinelibrary.com.]

mass transfer. With the increase of viscosity ratios, the asymptotic Sherwood numbers Sh become smaller and smaller, which is 4.75 at $\lambda = 100$, quite close to 4.5 the known limit for a solid sphere.[4,10] Figure 8 implies higher mass transfer rates for a drop than for a solid sphere, indicating that the internal circulation of a drop readily

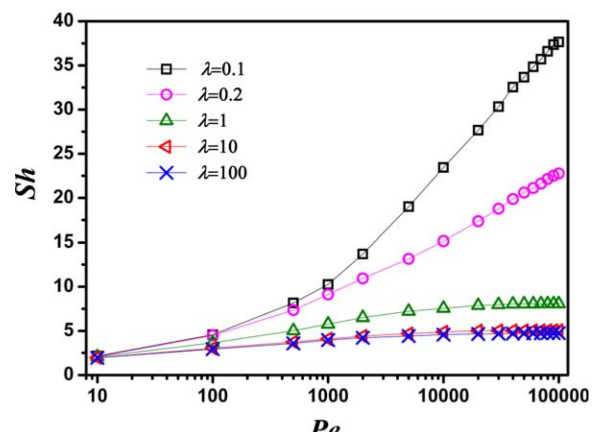

Figure 8. Variation of Sh with Pe_1 for mass transfer from a liquid drop in simple shear flow ($10 \le Pe_1 \le 100,000$).

[Color figure can be viewed in the online issue, which is available at wileyonlinelibrary.com.]

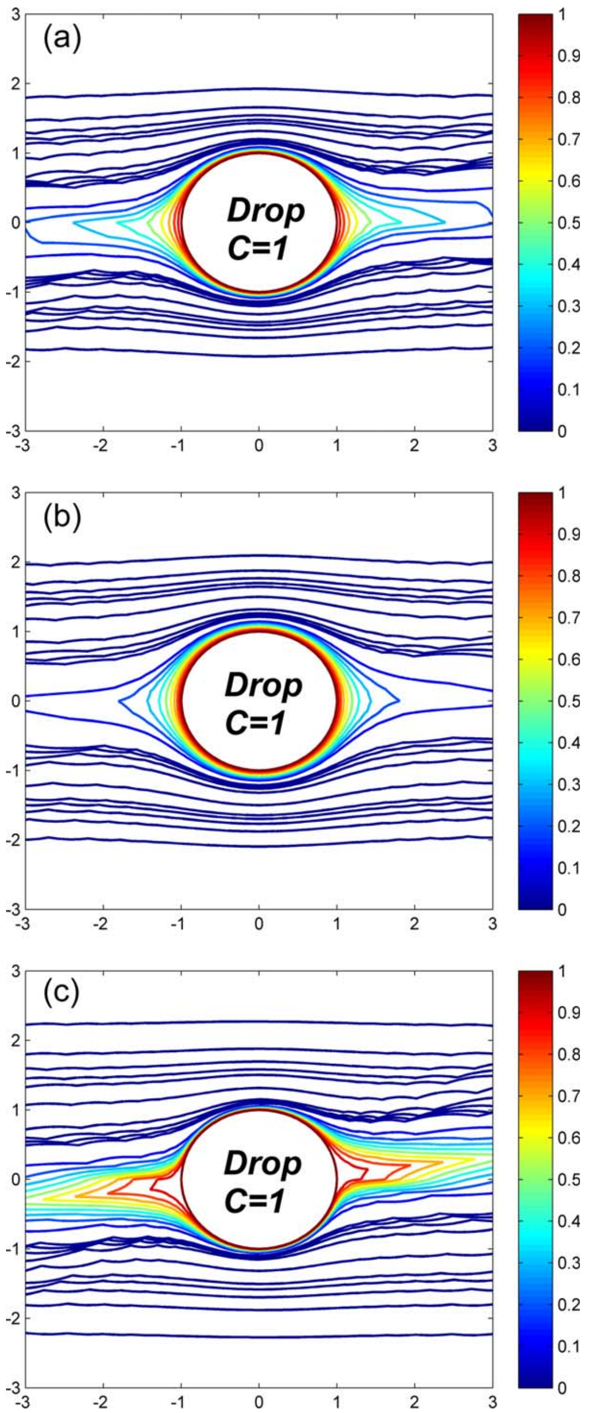

Figure 9. Contours of solute concentration around a liquid sphere in simple shear flow in *x-y* plane.

(a) $Pe_1 = 2000$, $\lambda = 0.1$; (b) $Pe_1 = 5000$, $\lambda = 1$; (c) $Pe_1 = 50{,}000$, $\lambda = 10$. [Color figure can be viewed in the online issue, which is available at wileyonlinelibrary.com.]

promotes the process of mass transfer even when internal transport resistance is negligible, an interesting result.

Based on the present simulations, the following correlation is proposed for predicting Sh in the range of $1000 \leq Pe_1 \leq 100,000$ with relative errors less than 4%

$$Sh = \frac{-40.3 + 9.15\ln Pe_1 - 0.3(\ln Pe_1)^2 + 29\lambda}{1 - 0.079\ln Pe_1 + 6.3\lambda} \tag{23}$$

When Peclet number is very large, the concentration contours will become more condensed near the surface of the liquid drop because of extensive convection. Figure 9 depicts the concentration profiles near a fluid sphere in simple shear creeping flow at different Pe_1, which are consistent with the distribution of the first-order derivative of the scalar C in Figure 3b. It is observed that the topology of concentration contours become more and more similar to the topology of the streamlines with increasing Pe_1, which results from the dominance of the convection over the diffusion. In addition, the boundary layer of concentration becomes thinner as Pe_1 increases.

Mass transfer inside a liquid sphere

For uniform or extensional creeping flows,[1,17] the circulating velocity inside the drop are proportional to $1/(\lambda+1)$. Therefore, the relationships between Sh and $Pe_2/(\lambda+1)$ are investigated. For the simple shear creeping flow, however, this is not the case, for $u_{2\varphi}$ is not directly proportional to $1/(\lambda+1)$ as shown by Eq. 9.

The mass transfer inside a liquid sphere without resistance in the surrounding fluid is a transient process, in which the internal concentration of the solute reduces to zero as well as Sh decreases to an asymptotic value gradually. Figure 10

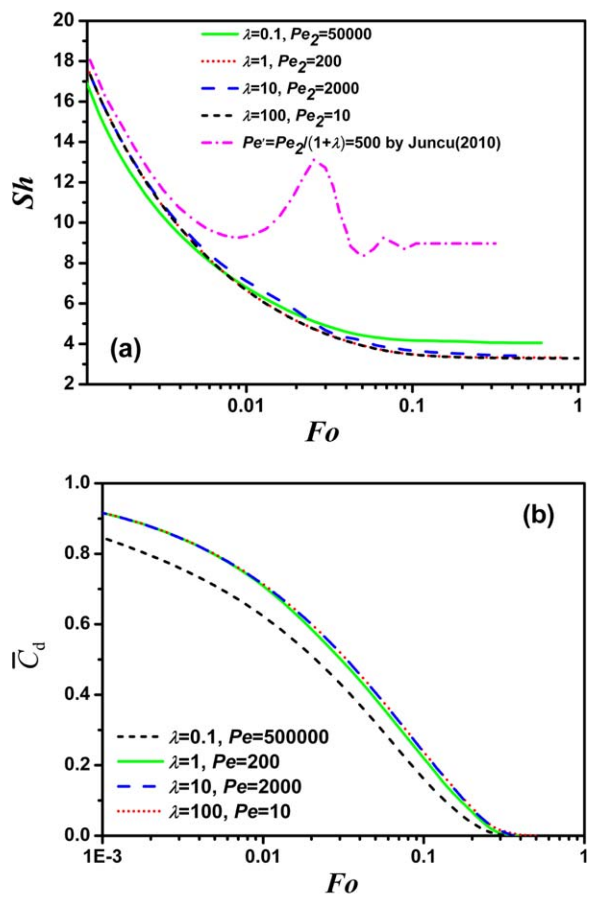

Figure 10. Transient transport behavior inside a liquid sphere in simple shear flow.

(a) *Sh* vs. *Fo*; (b) $\overline{C}_d$ vs. *Fo*. [Color figure can be viewed in the online issue, which is available at wileyonlinelibrary.com.]

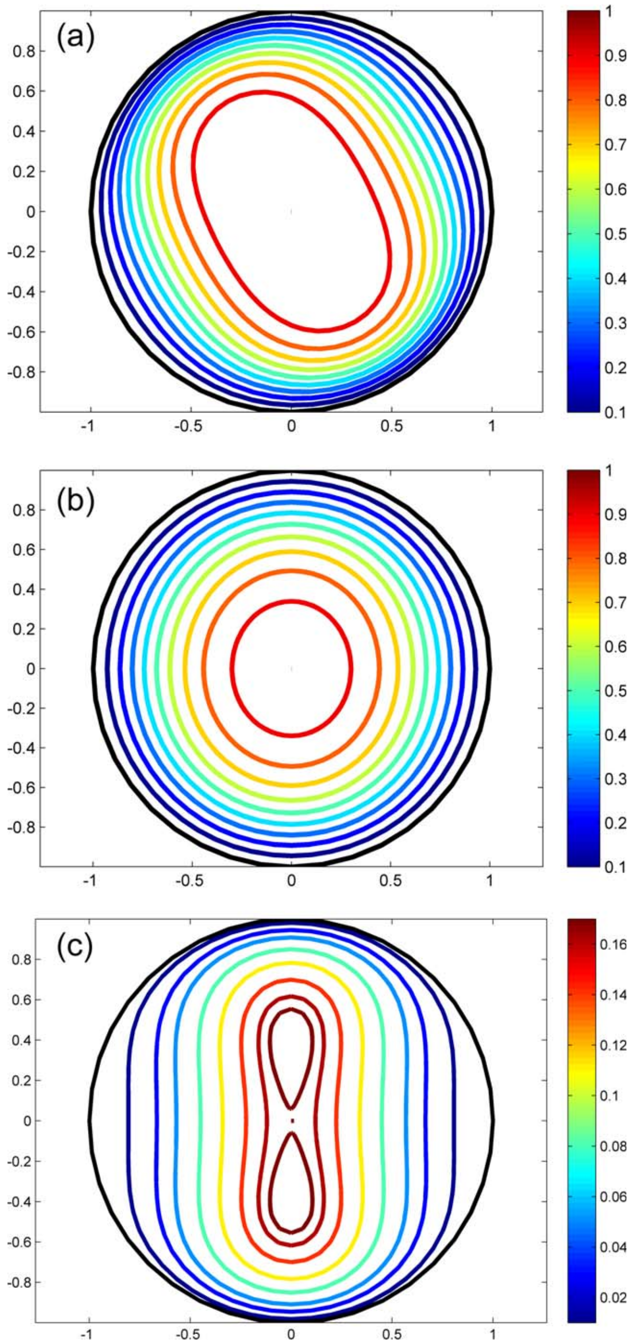

Figure 11. Contours of solute concentration inside a drop in simple shear flow in *x-y* plane.

(a) $Pe_2 = 50$, $\lambda = 1$, $Fo = 0.03$; (b) $Pe_2 = 5000$, $\lambda = 10$, $Fo = 0.05$; (c) $Pe_2 = 50{,}000$, $\lambda = 0.1$, $Fo = 0.17$. [Color figure can be viewed in the online issue, which is available at wileyonlinelibrary.com.]

depicts the variations of $\overline{C}_d$ and Sh with the dimensionless time namely the Fourier number $\left(Fo = \tau Pe_2^{-1} = D_2 t/a^2\right)$. For the transport processes in uniform or extensional flows,[1,2,17,23] Sh as a function of time would oscillate intensively for large Pe_2 and low viscosity ratios. Initially, the molecular diffusion dominates the transfer processes and Sh diminishes rapidly in time. But then, the fluid of high concentration from the inside is convected toward the outer surface. So Sh increases until a local maximum is achieved. This oscillating process would attenuate as the drop concentration decreases.[2] For simple shear flow, however, we found that Sherwood numbers decrease monotonically with increasing time, as shown in Figure 10a. This may result from the minor convective effect to mass transfer. In the whole transport process, the dominant diffusion effect thickens continuously the boundary layer of mass transfer, which leads to the reduction of the concentration gradient near the interface. According to Figure 10b, the reducing rate of $\overline{C}_d$ increases with time till Fo is about 0.1. After that, $\overline{C}_d$ goes through a point of inflexion: while $\overline{C}_d$ still decreases with increasing time and the reducing rate also decreases with increasing time and eventually approaches zero.

Figure 11 depicts the concentration evolution inside a liquid sphere at different Pe_2. Figure 11a gives a description of the concentration contours for intermediate Pe_2 in the initial time. Figure 11b indicates the concentration contours are almost analogous to those of the pure diffusion for high viscosity at a large Pe_2. As shown in Figure 11c, there are some small circulations inside the liquid sphere for low viscosity ratios, which is better for mass transfer. As a result, the transport rate at low viscosity ratios is higher than that at high viscosity ratios, analogous to the flow pattern in Figure 2b.

Figure 12 shows the variation in Sh with Pe_2 for several viscosity ratios. Sherwood numbers also approach asymptotic values, which are significantly less than those for uniform and extensional flows.[1,17] The reason may be that the multiple circulations in the latter flows could bring the solute from the interior of a drop to the inner surface of a drop. Hence, the convective effect for transport is greater than the case for the simple shear flow. In particular, the convective effect has negligible impact on the mass transfer for $\lambda = 10$ and $\lambda = 100$ at a wide range of Pe_2; Sherwood numbers are close to 3.29, the value for the pure diffusion situation. This is because the topology of streamlines is similar to a collection of concentric circles at high viscosity ratios; when the streamlines are nearly parallel to the surface of the drop and nearly parallel to the contours of concentration for the pure diffusion case, the effect of advection is small and the transport processes are dominated by diffusion. This is supported by Figure 4, where the distribution of the first-order derivative of C near the inner surface of the drop is almost invariant with respect to the internal circulation.

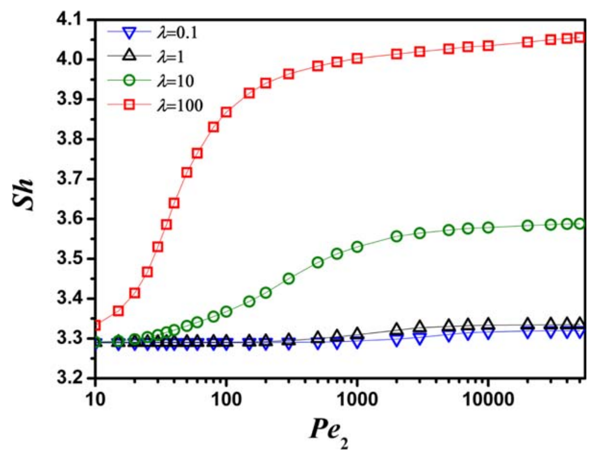

Figure 12. Variation of *Sh* with Pe_2 for a drop in simple shear creeping flow.

[Color figure can be viewed in the online issue, which is available at wileyonlinelibrary.com.]

Based on our simulations, one correlation applicable is proposed to predict Sh_∞ in the range of $10 \le Pe_2 \le 50,000$ and $0.1 \le \lambda \le 100$ with a maximum error of 6%

$$Sh_\infty = \frac{2.885 - 2.065 \ln Pe_2 + 0.470 (\ln Pe_2)^2 + 38.515\lambda}{1 - 0.634 \ln Pe_2 + 0.124 (\ln Pe_2)^2 + 11.703\lambda} \quad (24)$$

If a drop undergoes mass transfer for sufficiently long time, Sh would approach an asymptotic value Sh_∞ at last. It represents approximately the lower limit of mass transfer rate under certain conditions, so Eq. 24 can be used to describe the transport processes.

As mentioned, the Reynolds number is within the Stokes flow regime. Therefore, the increase in the Peclet number ($Pe = RePr$ or $ReSc$, where $Sc = \mu/(D\rho)$ and $Pr = \mu C_t/k$) means that Pr (or Sc) will go to very large values, corresponding to very low values of mass (or thermal) diffusivity. Therefore, although the correlations (Eqs. 20, 23, and 24) are functions of Peclet number, they represent the effect of Pr (or Sc) on Nu (or Sh) in creeping flow only. All above graphs and correlations on mass transfer apply analogously to heat transfer, just by replacing Sh with Nu and Sc with Pr and so forth.

Conclusions

In terms of the known Stokes velocity field at small Reynolds numbers, steady-state mass/heat transfer outside a liquid sphere and transient transport inside a liquid sphere in simple shear creeping flow are investigated by numerical simulations.

For the external transport problem, our simulations show that Sh would reach an asymptotic value for sufficiently large Pe_1 at any viscosity ratio, which is related with the closed streamlines around the sphere. The value of viscosity ratio also influences the rate of mass transfer. When $\lambda = 100$, the transport behavior is close to that of solid spheres. This characteristic asymptotic value differs substantially from the case in uniform or extensional flows.

For the transient internal problem inside a liquid sphere, the simulation results indicate that Sh also approaches an asymptotic value. However, the convective effect is weak on the mass transfer inside the sphere at high viscosity ratios, which is related to the special topology of streamlines.

Based on our simulation data, two new empirical formulas are built. Eq. 22 can be used to predict Sh at $1000 \le Pe_1 \le 100,000$ and $0.1 \le \lambda \le 100$ with acceptable errors for the steady mass/heat transfer from a liquid sphere. For the unsteady transport process, Eq. 23 can predict Sh_∞ in range of $10 \le Pe_2 \le 50,000$ and $0.1 \le \lambda \le 100$ with a maximum error of 6%.

This study deals with shear flow around an isolated drop. The present results are useful for the dilute suspensions with insignificant settling that are mostly relevant for mist and aerosol situations. In other applications, shear plus slip may be a more realistic situation. The physical problem of the synergistic effect of shear and slip should consider the relative directions of the shear and the slip flows and the ratio of the shear rate to the slip velocity, and it is a problem that requires much more effort to be fully characterized and comprehended.

Notation

a = drop radius, m
c = dimensional concentration, mol/m^3
C = dimensionless concentration
$\overline{C}_d$ = dimensionless average concentration in the drop
C_t = heat capacity, J/K
D = diffusivity, m^2/s
$\mathbf{E}$ = rate–of–strain tensor
Fo = Dt/a^2, Fourier number
h = heat transfer coefficient, J·m^{-2}·s^{-1}·K^{-1}
K_t = thermal conductivity, J·m^{-1}·s^{-1}·K^{-1}
k = mass transfer coefficient, m/s
N = number of grid
Nu = ka/D, Nusselt number
Pe = $\dot{\gamma}a^2/D$, Peclet number
Pr = $\mu C_t/k$, Prandtl number
r = dimensionless radial coordinate
$\mathbf{r}$ = position vector, m
R = size of dimensionless computing domain
Sc = $\mu/(D\rho)$, Schmidt number
Sh = Sherwood number, defined in Eq. 18
t = time, s
u = flow velocity, m/s
$\mathbf{u}$ = velocity vector, m/s

Greek letters

α = thermal conductivity, m^2/s
$\dot{\gamma}$ = characteristic magnitude of velocity gradient
$\mathbf{\Gamma}$ = transpose of velocity gradient tensor
θ = spherical polar angle, rad
λ = interior-to-exterior viscosity ratio
μ = viscosity, Pa·s
ρ = density, kg·m^{-3}
τ = $\dot{\gamma}t$, dimensionless time
φ = spherical azimuthal angle, rad
$\mathbf{\Omega}$ = vorticity tensor

Superscripts

s = drop surface

Subscripts

0 = initial state or center of droplet
1 = continuous phase
2 = drop
∞ = far from the drop or finite large time
r = spherical radial component
θ = spherical polar component
φ = spherical azimuthal component

Acknowledgments

This work was supported by the National Basic Research Program of China (2012CB224806), the National Science Fund for Distinguished Young Scholars (21025627), the National Natural Science Foundation of China (20990224, 21106154), 863 project (2012AA03A606) and CAS Program for Cross & Cooperative Team of the Science and Technology Innovation. The authors thank Professor Donald L. Koch at Cornell University for his useful discussions on this work.

Literature Cited

1. Clift R, Grace JR, Weber ME. Bubbles, Drops, and Particles. New York: Academic Press, 1978.
2. Sadhal SS, Ayyaswamy PS, Chung JN. Transport Phenomena with Drops and Bubbles. Berlin: Springer, 1996.
3. Frankel NA, Acrivos A. Heat and mass transfer for small spheres and cylinders freely suspended in shear flow. *Phys Fluids*. 1968;11: 1913–1918.

4. Acrivos A, Heat transfer at high peclet number from a small sphere freely rotating in a simple shear field. *J Fluid Mech.* 1971;46:233–240.
5. Robertson CR, Acrivos A. Low Reynolds number shear flow past a rotating circular cylinder. Part 1. Momentum transfer. *J Fluid Mech.* 1970;40:685–704.
6. Robertson CR, Acrivos A. Low Reynolds number shear flow past a rotating circular cylinder. Part2. Heat transfer. *J Fluid Mech.* 1970; 40:705–718.
7. Subramanian G, Koch DL. Centrifugal forces alter streamline topology and greatly enhance the rate of heat and mass transfer from neutrally buoyant particles to a shear flow. *Phys Rev Lett.* 2006;96:134503.
8. Subramanian G, Koch, DL. Inertial effects on the transfer of heat or mass from neutrally buoyant spheres in a steady linear velocity field. *Phys Fluids.* 2006;18:073302.
9. Subramanian G, Koch DL, Zhang JS, Yang C. The Influence of the inertially dominated outer region on the rheology of a dilute of low-reynolds-number drops or rigid particles. *J Fluid Mech.* 2011;674:307–358.
10. Yang C, Zhang JS, Koch DL, Yin XL. Mass/Heat transfer from a neutrally buoyant sphere in simple shear flow at finite Reynolds and Peclet numbers. *AIChE J.* 2011;57:1419–1433.
11. Leal LG. On the effective conductivity of a dilute suspension of spherical drops in the limit of low particle Peclet number. *Chem Eng Commun.* 1973;1:21–31.
12. Li R, Zhang JS, Yong YM, Wang Y, Yang C. Numerical simulation of steady flow past a liquid sphere immersed in a simple shear flow at low and moderate Re. *Chin J Chem. Eng.* In press.
13. Bartok W, Mason SG. Particle motions in sheared suspensions. VII. Internal circulation in fluid droplets (theoretical). *J Colloid Sci.* 1958;13:293–307.
14. Peery JH. Fluid mechanics of rigid and deformable particles in shear flow at low Reynolds numbers Ph.D. Thesis. Princeton University, Princeton, NJ 1966.
15. Yang C, Mao ZS. Numerical simulation of interphase mass transfer with the level set approach. *Chem Eng Sci.* 2005;60:2643–2660.
16. Leal LG. Laminar Flow and Convective Transport Processes. London: Butterworth-Heinemann, 1992.
17. Zhang JS, Yang C, Mao ZS. Mass and heat transfer from or to a single sphere in simple extensional creeping flow. *AIChE J.* 2012;58: 3214–3223.
18. Zhang YH, Yang C, Mao ZS. Large eddy simulation of liquid flow in a stirred tank with improved inner-outer iterative algorithm. *Chin J Chem Eng.*, 2006;14:321–329.
19. Feng ZG, Michaelides EE. Mass and transfer from fluid spheres at low Reynolds numbers. *Powder Technol.* 2000;112:63–69.
20. Bowman CW, Ward DM, Johnson AI, Trans O. Mass transfer from fluid and solid spheres at low Reynolds numbers. *Can J Chem Eng.* 1961;39:9–13.
21. Newman AB. The drying of porous solid: diffusion and surface emission equations. *Trans Am Inst Chem Eng.* 1931;27:203–213.
22. Kronig R, Brink JC. On the theory of extraction from falling droplets. *Appl Sci Res.* 1950;A2:142–154.
23. Juncu G. A numerical study of the unsteady heat/mass transfer inside a circulating sphere. *Int J Heat Mass Transfer.* 2010;53:3006–3012.

Manuscript received Dec. 28, 2012, revision received July 7, 2013, and final revision received Sept. 16, 2013.